RESEARCH ARTICLE
doi: 10.2306/scienceasia1513-1874.2025.s021

ScienceAsia 51S (2): 2025: ID 2025s021: **1–8**

Geometrical approach for identifying the corners of convex bodies composed by circular arcs

Asama Jampeepan[a,*], **Supanut Chaidee**[b], **Papangkorn Inkeaw**[c]

[a] Program in Applied Mathematics, Department of Mathematics, Faculty of Science, Chiang Mai University, Chiang Mai 50200 Thailand

[b] Advanced Research Center for Computational Simulation (ARCCoS), Department of Mathematics, Faculty of Science, Chiang Mai University, Chiang Mai 50200 Thailand

[c] Data Science Research Center, Department of Computer Science, Faculty of Science, Chiang Mai University, Chiang Mai 50200 Thailand

[*]Corresponding author, e-mail: AsamaCMU@gmail.com

Received 1 Dec 2024, Accepted 9 Sep 2025
Available online 20 Dec 2025

ABSTRACT: This paper presents a mathematical approach for accurately identifying the iris boundaries in photographic pictures, specifically focusing on eye position detection. This issue is of significance for several applications, especially in the field of eye tracking. Suppose that the detected data of the iris combined with eyelids is given. We assumed that the shape of the detected data is represented by the boundary of a convex body composed of circular arcs that represent the boundaries of the iris, upper eyelid, and lower eyelid. The objective is to identify the iris boundary from generated points on the boundary of the convex body corresponding to the position of gaze. We investigate the geometric properties of convex bodies, specifically focusing on their corners, which are non-differentiable points. An algorithm is then established to classify points to the iris boundary or the eyelids. This is done by utilizing convex hull and exterior angle analysis. The set of finite points around the boundary of the iris can be used to approximate the center of the iris. The experiments were conducted using both ideally generated data and real data obtained from photographic images of eyes.

KEYWORDS: convex body, corner point, non-differentiable point, discrete curvature, exterior angle

MSC2020: 52B55 52C05 68U05

INTRODUCTION

The problem of detecting the desired points from photographic images is currently being widely studied in various fields, such as computer vision [1] and Artificial Intelligence (AI) [2]. In this era, researchers use advanced algorithms and machine learning models to classify data sets, focusing on individual data points. AI, clustering and classification techniques are used, and ongoing research is designed to improve the robustness and scalability of the algorithm [3].

A significant application related to data point classification is gaze position detection, commonly known as eye tracking, which is crucial to addressing various medical problems [4]. It helps in diagnosing neurological disorders, studying eye movements, and assessing cognitive function [5]. In estimating gaze position, circle fitting algorithms are widely used [6]. This technique involves capturing an image of the eye, identifying the iris boundary, and extracting data points from this boundary. Subsequently, these extracted data points are used in circle-fitting algorithms to find the best-fit circle.

Currently, many algorithms have been designed to determine the best-fit circle for a given set of data points. These algorithms can be classified into two main types [7]: geometric fitting and algebraic fitting. As compiled in the previous study [7], the study investigated the efficiency and reliability of algebraic and geometric approaches in computational mathematics. It found that algebraic methods can lead to calculation problems due to numerical errors, while geometric approaches offer more robust and efficient solutions. Geometric algorithms are noted for their clarity, understandability, and ability to provide better approximations in computations, making them a preferable choice in certain applications. Especially for an object with a clearly defined shape, an analysis grounded on its precise shape would provide more accurate results.

In the case of a convex body composed of circular arcs, in addition to the consideration of discrete data, the exterior angle of the discrete curvature can be used as a mathematical tool to identify the corners of a convex body. These corner points serve as separators for classifying the datasets. Once the data points are determined, an appropriate algorithm can be employed to fit a circle accurately.

The main purpose of this study is to identify the boundary of the iris by generating points on a convex body made up of circular arcs. The modeling assumptions are based on gaze positions, as detailed in the study [8]. We mathematically investigate the geometric properties of the convex body, focusing on its corners, which are referred to as non-differentiable

points. Next, we compute the convex hull of the points on the convex body to analyze the behavior of the exterior angles. Finally, we classify the data points on the convex hull using statistical criteria to extract the desired data, which is then used to fit a circle to both ideally generated and real-world data points.

PRELIMINARIES

In this study, we focus on the analysis of geometric shapes, including fundamental aspects of convex polygons and computations that involve polygons, convex sets, and convex hulls. Additionally, we explore the geometric properties for detecting non-differentiable points of a convex body together with the problem formulation.

Basic concepts in geometry

The primitive object in discrete and computational geometry is a polygon, a region on a plane enclosed by a finite collection of line segments, which forms a simple closed curve. We define a subset S of the plane as *convex* if, for any two points x and y within S, the line segment $\overline{xy}$ that connects them entirely within S. Especially in the case of convex polygon, we consider that it is a polygon whose each internal angle is at most π. Essentially, the vertices of a convex polygon extend outward, with no sides pointing inward.

If the set S is given, we find the convex hull of S, the smallest convex set that contains S, denoted as $\mathscr{CH}(S)$. It can be seen as the intersection of all convex sets that cover S. For a given finite point set S, various algorithms compute the convex hull of S, such as Graham's scan algorithm [9] and the divide-and-conquer algorithm [10]. It is notable that the lower bound of complexity for computing a convex hull is proved to be $\Omega(n \log n)$, where n is the number of given points. The result of computing the convex hull of S is a convex polygon containing S.

The relationship between interior and exterior angles begins with the concept of an interior angle, which is formed by two sides of a polygon sharing a common vertex. In the case of a triangle, there are three interior angles, and their measures sum to 180°. The sum of the measures of the interior angles of a convex polygon with n sides is $(n-2)180°$.

On the other hand, an exterior angle is formed by extending one side of a polygon and considering the angle between this extension and an adjacent side. The exterior angles form linear pairs with their corresponding interior angles. Furthermore, a remote interior angle is an interior angle that is not adjacent to the exterior angle.

In this study, we focus on the exterior angle of a vertex of a convex polygon in terms of discrete curvature. Let $\mathscr{P}$ be a convex polygon in $\mathbb{R}^2$ with vertices $v_1, v_2, \ldots, v_n$ such that $v_i = (x_i, y_i)$, where n is the number of vertices of the convex polygon and assume $v_n = v_0$ and $v_{n+1} = v_1$. At each vertex v_i, the exterior angle θ_i is defined as the angle between consecutive tangent vectors $\overrightarrow{T}_{i-1}$ and $\overrightarrow{T}_i$:

$$\theta_i = \arccos\left(\overrightarrow{T}_{i-1} \cdot \overrightarrow{T}_i\right), \tag{1}$$

where the unit tangent vector at vertex v_i is denoted by $\overrightarrow{T}_i := \frac{\overrightarrow{e}_i}{\|\overrightarrow{e}_i\|} = \frac{v_{i+1}-v_i}{\|v_{i+1}-v_i\|}$ for $i = 1, 2, \ldots, n$, and the vector $\overrightarrow{e}_i := v_{i+1} - v_i$ denotes the edge vector from vertex v_i and v_{i+1}.

Modeling assumptions

The aim of this study is to find the best fit circle that satisfies the shape of the iris boundary, as shown in Fig. 1 (left).

Based on the observation of the previous study [8], there are nine positions of gaze as illustrated in Fig. 2.

To simplify this problem, we consider the recognized shape as a convex body composed of circular arcs, as shown in Fig. 2. We assume that the circle can be truncated to a maximum of three curves: C_1, C_2, and C_3. Based on gaze positions, we categorize the data patterns into four distinct groups, as shown in Fig. 3. Each group represents a pattern of gaze behavior observed in our study.

For the assumed shape, the different curves are composed of the boundary of a convex body, and non-differentiable points, which are the corners of the convex body, are recognized. We aim to obtain the circle of the curve C_1 whose radius is minimum, that is, C_1 has the largest curvature. In practice, the information obtained from the real world would be discrete data. Therefore, we propose a deterministic algorithm to detect the corner points of the approximated convex shape to obtain the iris circle, both the center and the radius.

PROPERTIES OF CONVEX BODIES GENERATED BY CIRCULAR ARCS

In this section, we will explore how convex bodies are formed and investigate the properties of non-differentiable points on the boundary of a convex body, where the boundary is not a smooth curve.

Construction of convex body

We assume that the ideally generated data are produced on the convex body formed by the composition of circular arcs. Based on the modeling assumptions, the selection of the upper and lower eyelids would be circular arcs with a larger circle compared to the curve of the iris circle. Additionally, the center of the iris circle would be located in the region bounded by those curves. In the examples shown in Table 1, the radius of the iris circle is chosen as $r = 1$, while the radii of the circles of the upper and lower eyelids are $r = 2\sqrt{2}$, except in case (e) on the left, where the radius of the upper and lower eyelid circles is $r = 3$.

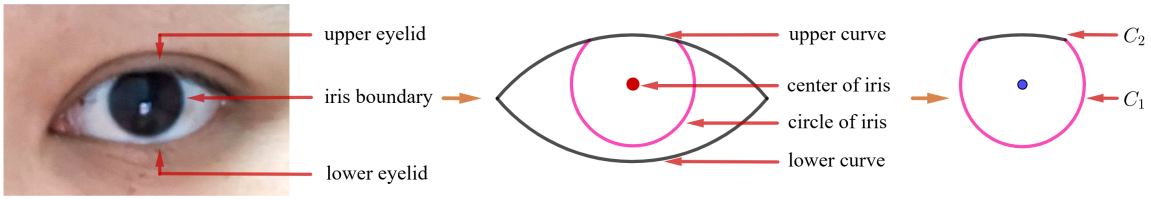

Fig. 1 Modeling procedure in this study: (left) an eye captured; (center) a model of the eye captured in geometric pattern; (right) the shape of convex body based on the position of circle of iris and curve C_2. The illuminated boundary represents the considered boundary of the convex body.

Table 1 An example of choosing the positions of the center in parts of convex bodies: the circle of the iris, the curve of the circle of the upper eyelid, the curve of the circle of the lower eyelid. Left and right indicate the sub-case of each gaze.

Gaze position in Fig. 2	Circle of the circular arc of iris		Circle of the circular arc of upper eyelid		Circle of the circular arc of lower eyelid	
	left	right	left	right	left	right
(a)	$(-1.1, 0.4)$	$(-1, \sqrt{7}-2)$	$(0,-2)$	$(0,-2)$	$(0,2)$	$(0,2)$
(b)	$(0, 2\sqrt{2}-2)$	$(0, 3-2\sqrt{2})$	$(0,-2)$	$(0,-2)$	$(0,2)$	$(0,2)$
(c)	$(1, \sqrt{7}-2)$	$(1.1, 0.4)$	$(0,-2)$	$(0,-2)$	$(0,2)$	$(0,2)$
(d)	$(-2, 0)$	$(-0.75, 0)$	$(0,-2)$	$(0,-2)$	$(0,2)$	$(0,2)$
(e)	$(0, 0)$	$(0, 0)$	$(0,-2)$	$(0,-2)$	$(0,2)$	$(0,2)$
(f)	$(0.75, 0)$	$(2, 0)$	$(0,-2)$	$(0,-2)$	$(0,2)$	$(0,2)$
(g)	$(-1.1,-0.4)$	$(-1,-(\sqrt{7}-2))$	$(0,-2)$	$(0,-2)$	$(0,2)$	$(0,2)$
(h)	$(0,-(2\sqrt{2}-2))$	$(0,-(3-2\sqrt{2}))$	$(0,-2)$	$(0,-2)$	$(0,2)$	$(0,2)$
(i)	$(1,-(\sqrt{7}-2))$	$(1.1,-0.4)$	$(0,-2)$	$(0,-2)$	$(0,2)$	$(0,2)$

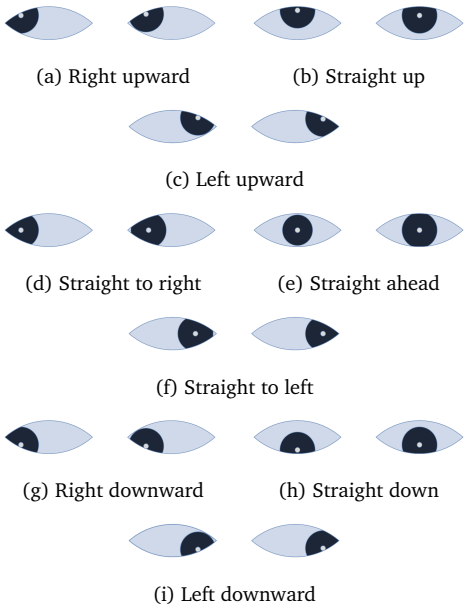

Fig. 2 The nine positions of gaze analyzed in this study.

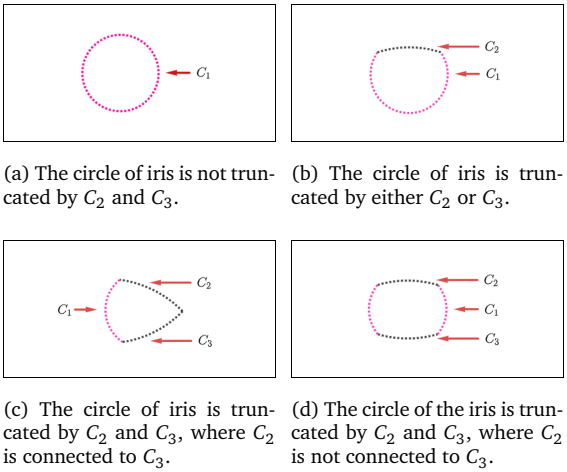

(a) The circle of iris is not truncated by C_2 and C_3.

(b) The circle of iris is truncated by either C_2 or C_3.

(c) The circle of iris is truncated by C_2 and C_3, where C_2 is connected to C_3.

(d) The circle of the iris is truncated by C_2 and C_3, where C_2 is not connected to C_3.

Fig. 3 Four distinct gaze behavior patterns based on truncation of the iris circle.

Investigation on properties of non-differentiable points

We have assumed that a convex body is composed of distinct circular arcs with different circle radii. The corner of the convex body is recognized as the non-differentiable point p that joins two curves C_i and C_j, as shown in Fig. 4.

To consider some discrete points on these curves, we assume that there are k_1 vertices $v_{1,1}, v_{1,2}, \ldots, v_{1,k_1}$ on the curve C_1 sorted clockwise and k_2 vertices $v_{2,1}, v_{2,2}, \ldots, v_{2,k_2}$, also sorted counterclockwise. Additionally, a point p is the vertex that joins these

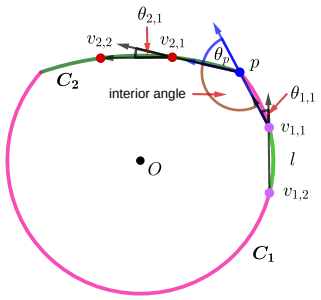

Fig. 4 An example of a convex body composed of circular arcs C_1 and C_2 used for the proof of Theorem 1.

two sequences, which is known to be the non-differentiable point of the two curves (or the corner of the convex body). Remark that each point in the pair of those vertices $v_{1,i}$ and $v_{1,i+1}$, and $v_{2,i}$ and $v_{2,i+1}$ has the same distance on each curve C_1 and C_2 with arc length l, where l is chosen sufficiently small. We then define a finite sequence of data points on the boundary of convex body as $\mathscr{C}_s = \{v_{1,k_1}, v_{1,k_1-1}, \ldots, v_{1,1}, p, v_{2,1}, v_{2,2}, \ldots, v_{2,k_2}\}$. From the sequence $\mathscr{C}_s$, we can derive the corresponding sequence of exterior angles:

$$\theta_s = \{\theta_{1,k_1}, \theta_{1,k_1-1}, \ldots, \theta_{1,1}, \theta_p, \theta_{2,1}, \theta_{2,2}, \ldots, \theta_{2,k_2}\},$$

where the exterior angle at each point is formed by the two tangent vectors at that point on the curve, and the sequence θ_s describes how the curvature of the boundary changes at each point.

In contrast to the problem setting, the information is obtained from an arbitrary exterior sequence. Therefore, we aim to find the point p in the given sequence to distinguish the smaller radius of the circle. To perform this procedure, it is necessary to investigate the geometric properties at the non-differentiable point p. Given a sequence of points on two different circular arcs (without loss of generality, all points are arranged in a counterclockwise direction), we detect the non-differentiable point to choose the appropriate circular arc for proceeding with circle fitting. In this context, the central angle θ of a circle is defined as the angle subtended at the center of the circle by an arc of length l, computed by $\theta = l/r$, where r is the radius of the circle. Using this definition, we can describe the properties of the convex body by the following lemma.

Lemma 1 *Given two circles c_1 and c_2, where c_1 has radius r_1 and c_2 has radius r_2 with $r_1 < r_2$. If a given arc length l on both arcs is equal, the central angle subtended by arc on c_1 is greater than the angle subtended by the arc on c_2.*

Proof: Noting that the arc length l on a circle is determined by the central angle θ and the radius r of the circle. Let θ_1 and θ_2 be the central angles subtended by the arc length l on circle c_1 and circle c_2, respectively. Then $\theta_1 := \frac{l}{r_1}$ and $\theta_2 := \frac{l}{r_2}$, which implies $\frac{l}{r_1} > \frac{l}{r_2}$, and it is concluded that $\theta_1 > \theta_2$. □

Lemma 2 *If the arc length of a circle is divided into segments of identical length, then all interior angles $\angle v_i v_{i+1} v_{i+2}$ on the arc of the circle will have the same measure, and so the exterior angles.*

Proof: Suppose that the circumference of the circle is equally divided into k parts with arc length l. We define a counterclockwise sequence of points in the circle by $\mathscr{C} = \{v_1, v_2, \ldots, v_k\}$ such that the central angle $\angle v_i O v_{i+1}$ is measured by $\theta = \frac{l}{r}$. Therefore, the interior angle $\angle v_i v_{i+1} v_{i+2}$ is equal to $\pi - \frac{l}{r}$. By equal subdivision, it is easy to see that the interior angles $\angle v_i v_{i+1} v_{i+2}$ for all $i = 1, 2, \ldots, k-2$ will also have the same measure. Recall the relationship between interior and exterior angles, which is given by:

$$\text{exterior angle} = \pi - \text{interior angle}.$$

Since all interior angles $\angle v_i v_{i+1} v_{i+2}$ are equal by assumption, exterior angles must also be equal. Therefore, the exterior angles at any point on the arc with the same arc length of the circle are equal. □

The following theorem is used to identify non-differentiable points.

Theorem 1 *Let the part of the boundary of a convex body be composed of circular arcs C_1 and C_2 with different circle radii. Given a sequence $\mathscr{C}_s$ of exterior angles, a point p on the arc C_1 and C_2 separates the circular arcs C_1 and C_2 if and only if the exterior angle of any arbitrary points on C_1 and C_2 with the same circular arc length differs from the exterior angle of p.*

Proof: Let C_1 and C_2 be arcs of circles with different radii r_1 and r_2, respectively. We firstly prove the necessary condition by assuming that p joins curve C_1 of circle c_1 and C_2 of circle c_2. We assume the sequence $\mathscr{C}_s$ as defined in previous part. Recall that $\mathscr{C}_s = \{v_{1,k_1}, v_{1,k_1-1}, \ldots, v_{1,1}, p, v_{2,1}, v_{2,2}, \ldots, v_{2,k_2}\}$ as shown in Fig. 4. By Lemma 2, the sub-sequence $\mathscr{C}_1 = \{v_{1,k_1}, v_{1,k_1-1}, \ldots, v_{1,1}\}$ on the curve C_1 generates the equal angles:

$$\begin{aligned}\angle v_{1,k_1} v_{1,k_1-1} v_{1,k_1-2} &= \angle v_{1,k_1-1} v_{1,k_1-2} v_{1,k_1-3} \\ &= \cdots = \angle v_{1,3} v_{1,2} v_{1,1}.\end{aligned}$$

Similarly, we have the same properties in the sub-sequence $\mathscr{C}_2 = \{v_{2,1}, v_{2,2}, \ldots, v_{2,k_2}\}$ as

$$\angle v_{2,1} v_{2,2} v_{2,3} = \angle v_{2,2} v_{2,3} v_{2,4} = \cdots = \angle v_{2,k_2-2} v_{2,k_2-1} v_{2,k_2}.$$

Without loss of generality, we would like to prove that $\angle v_{1,1} p v_{2,1}$ differs from $\angle v_{1,3} v_{1,2} v_{1,1}$

and $\angle v_{2,1}v_{2,2}v_{2,3}$. Lemma 2, it follows that the interior angles $\angle v_{1,3}v_{1,2}v_{1,1}$ and $\angle v_{2,1}v_{2,2}v_{2,3}$ are $\pi - \frac{l}{r_1}$ and $\pi - \frac{l}{r_2}$ such that $\frac{l}{r_1} > \frac{l}{r_2}$. We are now considering the form of the angle $\angle v_{1,1}pv_{2,1}$ by defining

$$\begin{aligned} v_{1,1} &= (r_1\cos\theta_1, r_1\sin\theta_1),\\ p &= \left(r_1\cos\left(\theta_1+\tfrac{l}{r_1}\right), r_1\sin\left(\theta_1+\tfrac{l}{r_1}\right)\right)\\ &= (r_2\cos\theta_2, r_2\sin\theta_2),\\ v_{2,1} &= \left(r_2\cos\left(\theta_2+\tfrac{l}{r_2}\right), r_2\sin\left(\theta_2+\tfrac{l}{r_2}\right)\right). \end{aligned}$$

Then we compute the interior angle $\angle v_{1,1}pv_{2,1}$ using $\cos\theta_p = \frac{\overrightarrow{v_{1,1}p}\cdot\overrightarrow{pv_{2,1}}}{\|\overrightarrow{v_{1,1}p}\|\|\overrightarrow{pv_{2,1}}\|}$, Therefore, we compute $\overrightarrow{v_{1,1}p}$,

$$\begin{aligned} \overrightarrow{v_{1,1}p} &= \langle r_1\cos\theta_1, r_1\sin\theta_1\rangle - \left\langle r_1\cos\left(\theta_1+\tfrac{l}{r_1}\right), r_1\sin\left(\theta_1+\tfrac{l}{r_1}\right)\right\rangle\\ &= \left\langle -2r_1\sin\left(\theta_1+\tfrac{l}{2r_1}\right)\sin\left(\tfrac{-l}{2r_1}\right), 2r_1\cos\left(\theta_1+\tfrac{l}{2r_1}\right)\sin\left(\tfrac{-l}{2r_1}\right)\right\rangle. \end{aligned}$$

Also

$$\begin{aligned} \overrightarrow{pv_{2,1}} &= \left\langle r_2\cos\left(\theta_2+\tfrac{l}{r_2}\right), r_2\sin\left(\theta_2+\tfrac{l}{r_2}\right)\right\rangle - \langle r_2\cos\theta_2, r_2\sin\theta_2\rangle\\ &= \left\langle -2r_2\sin\left(\theta_2+\tfrac{l}{2r_2}\right)\sin\left(\tfrac{l}{2r_2}\right), 2r_2\cos\left(\theta_2+\tfrac{l}{2r_2}\right)\sin\left(\tfrac{l}{2r_2}\right)\right\rangle. \end{aligned}$$

From $\overrightarrow{v_{1,1}p}$ and $\overrightarrow{pv_{2,1}}$, it follows that $\|\overrightarrow{v_{1,1}p}\|$ and $\|\overrightarrow{pv_{2,1}}\|$ equal to $2r_1\left|\sin\left(\frac{-l}{2r_1}\right)\right|$ and $2r_2\left|\sin\left(\frac{l}{2r_2}\right)\right|$, respectively. Therefore, the interior angle $\angle v_{1,1}pv_{2,1}$ is

$$\begin{aligned} \theta_p &= \arccos\left(\frac{\overrightarrow{v_{1,1}p}\cdot\overrightarrow{pv_{2,1}}}{\|\overrightarrow{v_{1,1}p}\|\|\overrightarrow{pv_{2,1}}\|}\right)\\ &= \arccos\left(\left\langle\sin\left(\theta_1+\tfrac{l}{2r_1}\right), -\cos\left(\theta_1+\tfrac{l}{2r_1}\right)\right\rangle\cdot\right.\\ &\quad\left.\left\langle -\sin\left(\theta_2+\tfrac{l}{2r_2}\right), \cos\left(\theta_2+\tfrac{l}{2r_2}\right)\right\rangle\right)\\ &= \arccos\left(-\cos\left(\tfrac{3}{2}\left(\tfrac{l}{r_1}-\tfrac{l}{r_2}\right)\right)\right). \end{aligned}$$

To prove that θ_p is different to θ_1 and θ_2, we claim that $\theta_p \neq \theta_1$ and $\theta_p \neq \theta_2$, where $\theta_1 = \pi - \frac{l}{r_1}$ and $\theta_2 = \pi - \frac{l}{r_2}$. We assume to choose l such that $\theta_p = \theta_1$ but $\theta_p \neq \theta_2$ or $\theta_p = \theta_2$ but $\theta_p \neq \theta_1$.They are trivial and follow directly from Lemma 1, i.e. if we choose l such that $\theta_p = \theta_1$ or $\theta_p = \theta_2$, it follow that $\theta_p \neq \theta_2$ or $\theta_p \neq \theta_1$, respectively. We then choose l such that $\theta_p \neq \theta_1$ and $\theta_p \neq \theta_2$. Remark that l_1, which yields $\theta_p = \theta_1$, satisfies

$$l_1 = \begin{cases} \frac{4\pi n r_1 r_2}{r_2 - 3r_1}, & r_2 \neq 3r_1 \text{ and } n \in \mathbb{Z}\\ \frac{4\pi(n+1) r_1 r_2}{5r_2 - 3r_1}, & 5r_2 \neq 3r_1 \text{ and } n \in \mathbb{Z}. \end{cases}$$

and l_2, which implies $\theta_p = \theta_2$, is considered by

$$l_2 = \begin{cases} \frac{4\pi n r_1 r_2}{3r_2 - 5r_1}, & 3r_2 \neq 5r_1 \text{ and } n \in \mathbb{Z}\\ \frac{4\pi(n+1) r_1 r_2}{3r_2 - r_1}, & 3r_2 \neq r_1 \text{ and } n \in \mathbb{Z}. \end{cases}$$

By considering $\theta_p = \theta_1$ and $\theta_p = \theta_2$, we can conclude that l can be chosen arbitrary, excepted in the case of l_1, l_2. Therefore, the interior angle $\angle v_{1,1}pv_{2,1}$ differs from $\angle v_{1,3}v_{1,2}v_{1,1}$ and $\angle v_{2,1}v_{2,2}v_{2,3}$, which implies the exterior angle also.

Conversely, it must be shown that if a value in the sequence of exterior angles differs at point p, then p is a separated point of curves C_1 and C_2.

From a given finite sequence $\mathscr{C}_s = \{v_{1,k_1}, v_{1,k_1-1}, \ldots, v_{1,1}, p, v_{2,1}, v_{2,2}, \ldots, v_{2,k_2}\}$, assume that each consecutive pair of points on the curve C_1 and C_2 has an arc length equal to l. Since the exterior angles at any point on the curve C_1 are all equal, and the exterior angles at any point on the curve C_2 are all equal, the curvature on the curve C_1 and C_2 are equal to $\frac{l}{r_1}$ and $\frac{l}{r_2}$, respectively. Without loss of generality, assume that $\frac{l}{r_1} < \frac{l}{r_2}$. Then there exists a real number θ_p such that $\frac{l}{r_1} < \theta_p < \frac{l}{r_2}$ which differs from $\frac{l}{r_1}$ and $\frac{l}{r_2}$. Therefore, p separate the boundary of convex body to arcs C_1 and C_2 as claimed. □

ALGORITHMS DESCRIPTION FOR DETECTING CORNER POINTS ON CONVEX BOUNDARIES

In this section, we present an algorithm to detect corner points in convex bodies formed by the composition of circular arcs. We assume that a set of discrete points S, which represents the boundary of a convex body, is given. It is important to note that the real-world data may not be perfectly convex. To address this, we compute the convex hull of S, denoted as $\mathscr{CH}(S)$. Next, we focus on identifying the corners of the shape. The goal is to classify the points into three categories: corner points, points on the eyelids, and points on the iris boundary. This classification is based on Theorem 1, which enables the identification of changes in exterior angles within sequences of exterior angles. The algorithm is outlined in Algorithm 1.

In this study, the number of points is determined by the pixel count along the circumference of the iris boundary. In all cases, the unit length is set in centimeters, with the iris radius fixed at 1 cm, corresponding to approximately 179 pixels along the circumference. For example, in case (e) left, the iris circle is complete and thus contains the full set of 179 points. In other cases, the point count depends on the arc length of the iris boundary, which varies according to gaze position (see Eq. (2)).)

We note that the choice of d from the set θ_s in Line 6 of Algorithm 1 depends on the features of the set. The default value is the third quartile (Q_3) of the set θ_s, which helps to effectively distinguish the sub-sequence. In practice, the detection of corner points might not be perfect, as proven in Theorem 1. However, it is promising to detect points where the exterior angles change.

Once the set θ_s is classified, we can obtain the

Algorithm 1 The Points Classification

Input: Sequence of boundary points S
Output: Set of corner points P, Set of sub-sequences of the eyelids E, Set of sub-sequences of iris boundary I.
Comment:
1. The positive number d depends on the set θ_s
2. Mean and SD are the average and standard deviation, respectively.

Construct $\mathscr{CH}(S)$.
Sort the point to the set $\mathscr{C}_s$ counterclockwise.
Append the first three members of $\mathscr{C}_s$ to $\mathscr{C}_s$.
For each three adjacent points in $\mathscr{C}_s$, compute exterior angle θ_i using (1), and append to the set θ_s.
Compute mean $\bar{\theta}_s$, SD, d of the set θ_s.
Compute Threshold $:= \bar{\theta}_s + d \cdot \mathrm{SD}$
for each $\theta_i \in \theta_s$ **do**
    if $\theta_i >$ Threshold **then**
        Add θ_i to set P (corner points)
    else if $\theta_i \geqslant \frac{l}{r_1}$ (in terms of pixels) **then**
        Add θ_i to set I (iris boundary)
    else
        Add θ_i to set E (eyelid points)
    end if
end for
Return the sets I, P, E

corresponding vertex sub-sequence of $\mathscr{C}_s$. We primarily focus on the set of iris boundary points to find the best-fit circle with respect to these points using existing algorithms, such as the least squares methods, RANSAC, and Pratt's method [7]. In this study, we simply employ the fitting using the fact of constructing the circle through three non-collinear points. Then, we choose any three points from the set I and construct the circle with respect to those three points. After that, we average the circles, including the center positions and radii, to obtain the appropriate circle.

EXPERIMENTAL RESULTS

Data

Given a set of points S in the plane, we first construct the convex hull $\mathscr{CH}(S)$ of these points in the experiment. Next, we sort the coordinates and calculate the exterior angle at each point of the convex hull $\mathscr{CH}(S)$ using the formula (1). Then, based on the statistical criteria mentioned in Algorithm 1, we separate the points. Therefore, the data points that are candidates for fitting a circle are obtained.

From the application viewpoint, a photo of the iris boundary is extracted as pixels instead of points on the plane. Therefore, we compute the reasonable number of points needed to generate the data points along the edge of the convex body. First, we calculate the number of ideally generated data points n. This involves determining the quantity of data by counting the pixels through which the circumference passes. To facilitate this calculation, we consider a circle with a radius of 1 centimeters, representing the iris, a circle with a radius of 3 (only in the case of (e) left), and $2\sqrt{2}$, which represents the upper and lower eyelids. Using Wolfram Mathematica for the conversion of centimeters to pixels (1 inch = 72 pixels), the number of pixels along the circumference C_{pixels}, is given by:

$$C_{\text{pixels}} = 2\pi r \times \frac{\text{number of pixels per inch}}{\text{number of centimeters per inch}}. \quad (2)$$

Therefore, the number of pixels along the circumference of a circle with radii $1, 3$, and $2\sqrt{2}$ is approximately 179, 504 and 535 pixels, respectively. For the frame of the ideally generated images, we assume that 1 cm $\approx$ 28.5 pixels, and the frame is 4×4 centimeters. Thus, the frame for each case is 114×114 pixels.

For real data, we extract data from eye images, focusing on the iris boundary and the curve of the eyelids. The data obtained consists of (x, y) coordinates in pixel format, with the frame size depending on the size of the collected images.

Experiments

For the case of ideally generated data, we first generate the data based on the cases identified in Fig. 2, which includes 18 sub-cases. We construct convex bodies and focus on the circle of the iris boundary in each case. Although the set of points on the circle is finite, the finite points of those parts are chosen based on the method mentioned above. The radius of the circle of the iris boundaries is the same, but the positions of these circles are chosen differently in each sub-case. In addition, the arcs of the eyelids in each sample are scaled according to the choice of the circle of iris boundaries.

We used Wolfram Mathematica 14.0 and employed the ConvexHullMesh command to compute the convex hull. Then we sort the coordinates, calculate the exterior angles to identify the corner points, and classify the data points into the iris boundary and the eyelid(s). The following figure shows the results obtained from fitting a circle to the ideally generated data after classifying the data.

To obtain the best-fit circle, we applied the average of circle passing through three points method, in which we computed the average of all circles uniquely defined by every combination of three distinct points from the set of iris boundary points.

For the case of real data, we collect the images [11] and detect facial features using Facial Keypoint Detection [12]. From the detected eye keypoints, a mask is created to isolate the eye region in the image. The Canny Edge Detection technique is then applied to extract the contour of the eye region, and the contour

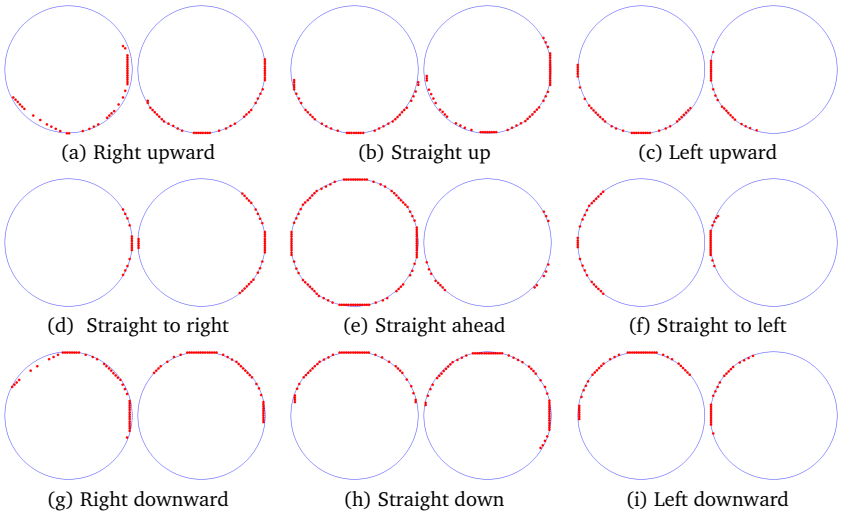

Fig. 5 Illustration of the nine positions of gaze analyzed in this study. Red points represent the points on the iris boundary obtained through classification.

Table 2 Comparison of initial and new center and radius values.

Gaze position in Fig. 2	Initial center	New center	Initial radius	New radius
(a) left	(25.65, 68.4)	(28.6884, 68.6586)	28.5	28.4481
(a) right	(28.5, 75.42)	(30.3741, 74.5569)	28.5	27.7394
(b) left	(57, 80.6)	(57.2964, 79.6017)	28.5	27.7290
(b) right	(57, 61.9)	(57.0775, 61.8975)	28.5	28.3623
(c) left	(85.5, 75.42)	(85.1940, 74.9435)	28.5	28.1055
(c) right	(88.35, 68.4)	(88.9411, 69.0086)	28.5	29.3245
(d) left	(0, 57)	(2.89641, 57.3362)	28.5	28.1723
(d) right	(35.625, 57)	(36.9830, 57.3792)	28.5	28.2237
(e) left	(57, 57)	(57.6126, 57.3874)	28.5	27.9871
(e) right	(57, 57)	(57.5380, 57.5916)	28.5	27.7276
(f) left	(78.375, 57)	(77.5685, 57.0601)	28.5	27.5620
(f) right	(114, 57)	(119.2640, 57.6741)	28.5	34.4820
(g) left	(25.65, 45.6)	(28.4980, 46.5952)	28.5	27.6684
(g) right	(28.5, 38.58)	(30.3466, 38.8884)	28.5	28.5162
(h) left	(57, 33.4)	(57.6558, 33.9775)	28.5	28.4314
(h) right	(57, 52.1)	(57.4745, 52.2943)	28.5	28.3334
(i) left	(85.5, 38.58)	(85.0845, 38.6054)	28.5	28.8066
(i) right	(88.35, 45.6)	(88.4231, 46.1163)	28.5	28.6845

coordinates are retrieved as pixel pairs. After obtaining the binary (black-and-white) image, Mathematica is used to extract the data points corresponding to the white regions, which represent the target data. These extracted points are subsequently processed following the steps described in Algorithm 1, similar to the procedure used for the ideally generated data. An example of fitting a circle to the classified data points is shown in Fig. 6.

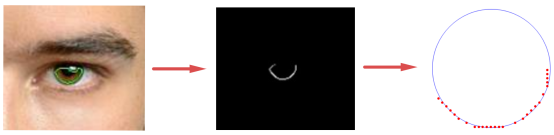

Fig. 6 An example of some process for fitting a circle to data points extracted from the image.

Results

From the experiments, the center and radius of the data were measured using a circle fitting algorithm. For the ideally generated data, we compared the solutions using Root Mean Square Error (RMSE). Let the initial center denoted by $c_i = (x_i, y_i)$ with radius r_i, and the corresponding new center and radius be $\hat{c}_i = (\hat{x}_i, \hat{y}_i)$ and $\hat{r}_i$, respectively, for $i = 1, \ldots, N$, where N is the number of all cases. The RMSE for the center

location is defined as

$$\mathrm{RMSE}_{\mathrm{center}} = \sqrt{\frac{1}{N}\sum_{i=1}^{N} \|\hat{\mathrm{c}}_i - \mathrm{c}_i\|_2^2} = \sqrt{\frac{1}{N}\sum_{i=1}^{N} [(\hat{x}_i - x_i)^2 + (\hat{y}_i - y_i)^2]}. \quad (3)$$

Similarly, the RMSE for the radius is given by

$$\mathrm{RMSE}_{\mathrm{radius}} = \sqrt{\frac{1}{N}\sum_{i=1}^{N} (\hat{r}_i - r_i)^2}. \quad (4)$$

The results yielded RMSE values of 1.97538 for the center and 1.50166 for the radius, indicating that the model provides a fairly accurate estimate of both. The higher RMSE for the center suggests a small error in its location, while the lower value for the radius shows good accuracy in size estimation. For real data, it is possible to fit a circle to the dataset. However, it is not possible to evaluate the error of the fitted circle relative to the size of the iris boundary, as the initial size of the iris boundary and the precise location of the center of the eye are unknown.

CONCLUSION REMARKS

This study modeled data points along the boundaries of convex bodies based on gaze positions and analyzed geometric properties to detect the corners of convex bodies. For data classification, the proposed method classified the data points into three categories: corner points, points on the iris boundary, and points on the eyelids. Regarding the circle-fitting algorithm, two types of data were considered: ideally generated data and real data. For the ideally generated data, the method performed well in fitting a circle due to the completeness of the data points. However, for the real data, some undesirable points were included in the approximation after classification. Thus, it was necessary to clean the data before applying the classification process.

For future work, we plan to validate this framework by applying it to real data obtained from the edges of the iris boundary. This will involve acquiring a dataset of actual iris images and addressing challenges such as undesirable points, lighting variations, and occlusions. The empirical validation will aim to refine the framework by improving data cleaning and classification processes, identifying limitations, and evaluating the performance of different circle fitting algorithms. These efforts will help provide informed recommendations for selecting the most suitable algorithm for practical applications in iris recognition.

Acknowledgements: The first author acknowledges the support of DPST, IPST, Ministry of Education, Thailand. Moreover, we thank Phapaengmueng Sukkasem for some of the discussions. The discussion for part of this project was also conducted in Geometry Boot Camp 2023–2024, especially with Supanat Kamtue. This research is partially supported by Chiang Mai University and the Data Science Research Center, Faculty of Science, Chiang Mai University.

REFERENCES

1. Kpalma K, Ronsin J (2007) An overview of advances of pattern recognition systems in computer vision. *Vis Syst*, 26.
2. ZHU WW, Berndsen A, Madsen EC, Tan M, Stairs IH, Brazier A, Lazarus P, Lynch R, et al (2014) Searching for pulsars using image pattern recognition. *Astrophys J* **781**, 117.
3. Mahdi MA, Hosny KM, Elhenawy I (2021) Scalable clustering algorithms for big data: A review. *IEEE Access* **9**, 80015–80027.
4. Moradizeyveh S, Tabassum M, Liu S, Newport RA, Beheshti A, Di Ieva A (2024) When Eye-tracking meets machine learning: A systematic review on applications in medical image analysis. *arXiv*, 2403.07834.
5. Ahmed IA, Senan EM, Rassem TH, Ali MA, Shatnawi HSA, Alwazer SM, Alshahrani M (2022) Eye tracking-based diagnosis and early detection of autism spectrum disorder using machine learning and deep learning techniques. *Electronics* **11**, 530.
6. Wang JG, Sung E (2002) Study on eye gaze estimation. *IEEE Trans Syst Man Cybern B Cybern* **32**, 332–350.
7. Chernov N, Lesort C (2005) Least squares fitting of circles. *J Math Imaging Vis* **23**, 239–252.
8. Lim HW, Lee DE, Lee JW, Kang MH, Seong M, Cho HY, Oh J-E, Oh SY (2014) Clinical measurement of the angle of ocular movements in the nine cardinal positions of gaze. *Ophthalmology* **121**, 870–876.
9. Golin M, Sedgewick R (1988) Analysis of a simple yet efficient convex hull algorithm. In: *Proceedings of the Fourth Annual Symposium on Computational Geometry*, pp 153–163.
10. Bærentzen JA, Gravesen J, Anton F, Aanæs H (2012) Convex hulls. In: *Guide to Computational Geometry Processing: Foundations, Algorithms, and Methods*, Springer, London, pp 227–240.
11. Gupta A (2020) Human faces: A web scraped dataset of human faces suggested for image processing models. Kaggle. Available at: https://www.kaggle.com/datasets/ashwingupta3012/human-faces.
12. Rosebrock A (2021) OpenCV face detection with Haar cascades. PyImageSearch. Available at: https://pyimagesearch.com/2021/04/05/opencv-face-detection-with-haar-cascades.